RSC Advances

PAPER

View Article Online
View Journal | View Issue

Cite this: *RSC Adv.*, 2015, **5**, 78655

Printed In-Ga-Zn-O drop-based thin-film transistors sintered using intensely pulsed white light†

Wi Hyoung Lee,[a] Seong Jun Lee,[b] Jung Ah Lim*[c] and Jeong Ho Cho*[b]

Received 10th July 2015
Accepted 10th September 2015

DOI: 10.1039/c5ra13573g

www.rsc.org/advances

We developed printed In-Ga-Zn-O (IGZO) thin film transistors (TFTs) by delivering droplets of a precursor solution using a picoliter fluidic dispensing system. Intensely pulsed white light (IPWL) was then used to sinter the printed deposits. From one to six drops, ring-like deposits with similar dimensions were formed; however, the morphologies and thicknesses of the deposits depended strongly on the droplet number. As the droplet number increased, the thickness of the IGZO thin film increased and the pile-up region at the periphery of the deposit gradually expanded. The electrical properties of the droplet-based IGZO TFT were strongly dependent on the droplet number and displayed the highest electron mobility and bias stability at three drops, which yielded good deposit thickness values both in the center and in the periphery regions of the ring-like deposits. These results will be useful for enhancing the electrical properties of TFTs based on printed IGZO films for use in the low-cost/flexible switching devices in display technologies.

1. Introduction

Thin film transistors (TFTs) based on metal oxide semiconductors have received significant attention as switching devices for use in display backplanes.[1] A variety of metal oxide semiconductors have been tested, and amorphous In-Ga-Zn-O (IGZO) has shown outstanding electrical properties, including high mobilities exceeding 10 $cm^2\ V^{-1}\ s^{-1}$ while maintaining purely amorphous characteristics.[2] The wide band gap (3.0 eV) of the film provided exceptionally transparent characteristics. In addition, a uniform film could be obtained at room temperature by using vacuum deposition techniques, such as sputtering or atomic layer deposition.[3] Thus, IGZO TFTs present an alternative to hydrogenated amorphous silicon TFTs for use in transparent/flexible TFTs on plastic substrates.

Although IGZO TFTs fabricated using vacuum deposition techniques are appealing as switching devices, their fabrication costs present a barrier to realizing low-cost printed electronics. Sol–gel processes involving an IGZO precursor solution would help reduce the preparation costs;[4] however, sol–gels require high-temperature annealing above 450 °C to remove organic ligand groups and activate the IGZO film properties. The sintering temperature may be reduced using a variety of approaches, such as modifying the precursor chemistry,[5] introducing combustion processing,[6] or photosintering using a light source (*i.e.*, excimer laser,[7] deep-ultraviolet,[8] flash light[9]) were proposed. Flash light photosintering annealing processes are advantageous as they provide rapid sintering within tens of milliseconds.[10] Intense pulsed white light (IPWL) can efficiently decompose organic ligands in a spin-cast IGZO precursor film, and IGZO TFTs have been successfully demonstrated using this technique.[9] Although spin-cast IGZO films provide uniform films over large areas, patterning processes are needed for certain device applications. Printing processes, such as inkjet printing, can provide patterned films within an area defined by a drop.[11–13] Inkjet printing, unfortunately, can be accompanied by processing problems, such as the formation of satellites, because solution dropping methods are non-contacting. Thus, we adopted contact-type picoliter fluidic dispensing system which was designed for printing a variety of organic and inorganic inks. The validity of this method was proposed by Larson *et al.*, who used ultrasonically driven micropipette to deposit small pattern with a dimension of several micrometers.[14]

In this study, we examined the morphological characteristics of IGZO deposits printed using a picoliter fluidic dispensing system. Ring-like films were successfully fabricated on substrates, and room-temperature sintering using IPWL was applied to remove the organic ligands. The droplet number, morphology, and thickness of the ring-like deposits were examined systematically. These morphological characteristics

[a]*Department of Organic and Nano System Engineering, Konkuk University, Seoul 143-701, Korea*

[b]*SKKU Advanced Institute of Nanotechnology (SAINT) and School of Chemical Engineering, Sungkyunkwan University, Suwon 440-746, Korea. E-mail: jhcho94@skku.edu*

[c]*Center for Opto-Electronic Materials and Devices, Post-Silicon Semiconductor Institute, Korea Institute of Science and Technology, Seoul 136-791, Korea. E-mail: jalim@kist.re.kr*

† Electronic supplementary information (ESI) available. See DOI: 10.1039/c5ra13573g

were correlated with the device performances of TFTs prepared using droplet-based IGZO deposits. The device operational stability, which is important for commercializing TFTs, was examined and a strong dependence on the drop number was observed.

2. Experimental details

The IGZO ink was prepared by mixing zinc acetate dehydrate, indium nitrate(III) hydrate, and gallium nitrate(III) hydrate in 2-methoxyethanol. The total concentration of the ink was 0.3 M, and the mole ratio of the atoms was adjusted to 2(In) : 1(Ga) : 1(Zn). A ring-type deposit was effectively formed on a SiO_2 (thickness of 300 nm)/Si substrate using a picoliter fluidic dispensing system. The deposited precursor was then sintered using an IPWL process conducted at a total irradiation energy of 100 J cm^{-2}. TFT devices were fabricated by depositing Ti (10 nm)/Au (70 nm) source/drain (S/D) electrodes (channel length = 100 μm channel width = 800 μm) onto the IGZO deposit. Printed morphologies of the IGZO deposits were characterized with optical microscope (Carl Zeiss) and surface profiler (Alpha-Step). Electrical properties of TFT devices were characterized using a semiconductor analyzer (Keithley 4200) at room temperature and ambient condition.

3. Results and discussion

Fig. 1a depicts a schematic diagram showing the picoliter fluidic dispensing system and IPWL process used to fabricate IGZO droplets. The IPWL process was found to effectively remove carbonyl, nitrate, and hydroxyl functional groups, as explained previously.[9] An optical microscopy image of a deposit formed using one droplet of an IGZO solution is shown in Fig. 1b. Because the diameter of the deposit exceeded the channel width of the S/D electrodes, the active channel region was defied within the deposit (Fig. 1b).

Fig. 2a–f show optical microscopy images of the deposits prepared from the IGZO droplets with various droplet numbers after sintering using the IPWL process. The image of the deposit obtained from one droplet revealed a uniform central region with a certain degree of pile-up at the periphery of the deposit (Fig. 2a). This pile-up is typical in inkjet printing processes and could be explained as resulting from the coffee staining effect caused by convective flow at the pinned droplet.[15] Interestingly, a wavy structure was observed at the deposit edge that may have

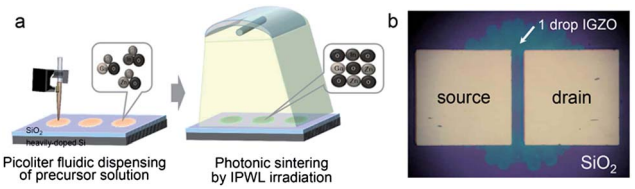

Fig. 1 (a) Schematic showing IPWL process of printed IGZO droplet. (b) Optical microscopy image of amorphous IGZO TFT with one droplet of IGZO solution.

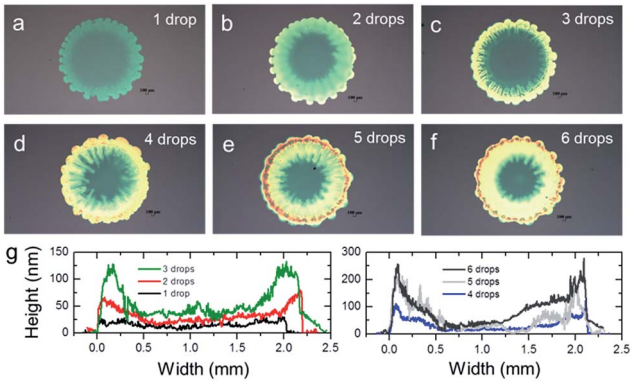

Fig. 2 Optical microscopy images of printed IGZO deposits from droplets with various drop numbers: 1 drop (a), 2 drops (b), 3 drops (c), 4 drops (d), 5 drops (e), 6 drops (f). (g) Surface profiles of the IGZO deposits.

resulted from a Marangoni-like instability caused by the surface tension gradient. A concentration gradient at the edge can lead to surface tension-driven Marangoni-like instabilities. As the droplet number increased (from one drop to three drops), the pile-up effects at the periphery increased (see the surface profiles shown in Fig. 2g). In addition, the height of the central region increased from 10 nm (one drop) to 20 nm (two droplets), and 30 nm (three drops), respectively. On the other hand, the dimensions of the deposit did not change with the droplet number. As a new droplet was dispensed at the position of the dried deposit, solvent evaporation in the new droplet occurred within the preformed structure of the former deposit. Thus, the ring-like deposit did not change in its dimension; rather, the preformed structure provided an efficient microwell that induced convective flow-induced coffee-staining effects that increased the thickness of the pile-up at the periphery of the deposit. Larger drop numbers (4, 5, 6 drops) produced a deposit in which the pile-up at the edge extended toward the center region of the ring-like deposit (see Fig. 2d–f). The surface profile shown in Fig. 2g reveals the gradual intrusion of the pile-up; thus, the diameter of the uniform region at the center was less than 1 mm. The sequential deposition of the droplet at a given position relies on this expansion of the pile-up region as an indispensable feature of the evaporation process, in which a new droplet is contained within a preformed microwell. Because the dimensions of the ring-like deposit were nearly identical and the IPWL-annealed IGZO deposit was purely amorphous in structure, as reported previously,[9] comparative analysis of TFT characteristics with drop-based IGZO active layer is possible.

Fig. 3a shows the transfer characteristics of IGZO drop-based TFTs with various drop numbers (from one drop to five drops). The ON current increased as the drop number increased from one drop to three drops. On the other hand, the ON current decreased as the drop number increased from three drops to five drops. The OFF current remained nearly the same, regardless of the drop number. The field-effect mobility was calculated according to the following equation.

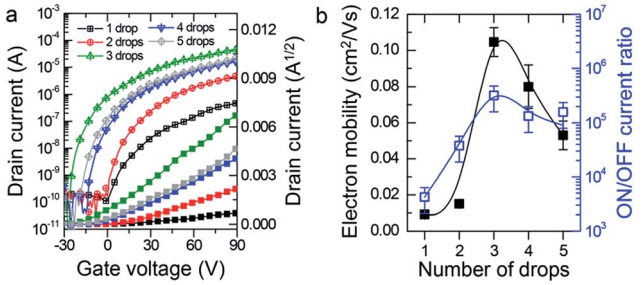

Fig. 3 (a) Transfer characteristics of IGZO TFTs with various drop numbers of IGZO solution. (b) Plots of electron mobility and ON/OFF current ratio *versus* number of droplets.

$$I_{DS} = \frac{WC_i}{2L}\mu(V_{GS} - V_T)^2,$$

where $C_i = 1.08 \times 10^{-8}$ F cm^{-2}, $W = 800$ μm, and $L = 100$ μm. The average electron mobilities and the ON/OFF current ratios extracted from the transfer characteristics measured from 10–15 devices are shown in Fig. 3b. All the device characteristics were summarized in Table 1. The average electron mobility in the TFTs prepared with one drop of IGZO was quite low (0.009 cm^2 V^{-1} s^{-1}). The TFTs prepared with three drops of IGZO, however, yielded an average electron mobility of 0.1 cm^2 V^{-1} s^{-1}, more than one order of magnitude higher than the electron mobility obtained from a single drop. As the drop number increased, the average electron mobility and the ON/OFF current ratio decreased. This trend could be explained by considering the morphology of the printed deposit obtained from the IGZO solution. The printed deposits prepared with 1–3 drops yielded a uniform central region with a diameter exceeding 1 mm (see the color contrast and height profiles in the optical microscopy (OM) images shown in Fig. 2a–c), which exceeded the width of the S/D electrodes (800 μm). Thus, only the central region contributed to the observed electrical properties. Fig. 2g left clearly reveals an increase in height in the central region (10 nm for one drop, 20 nm for two drops, 30 nm for three drops). It has been reported that thickness of an IGZO active layer is critical to the electrical performances of IGZO TFTs.[16–20] Although there exist debates on the optimum thickness of an IGZO active layer, layers thicker than 30 nm were necessary for both the sputtered and printed IGZO TFTs.[18,19] Thus, the improved electrical properties (from one drop to three drops) resulted from an increase in the thickness of the printed IGZO layer. Charge transport in thinner IGZO films tended to suffer from the adverse effects of a higher surface roughness.[19]

On the other hand, subthreshold slope decreased with an increase of drop number (from one drop to three drops). Subthreshold slope can be used for measuring trap density by using the following equation.

$$N_{trap}^{max} = \frac{C_i}{q}\left[\frac{qS\log e}{kT} - 1\right]$$

where C_i is the capacitance of SiO_2 (1.08×10^{-8} F cm^{-2}), q is the electronic charge, S is the subthreshold slope (V dec^{-1}), and k is Boltzmann's constant (1.38×10^{-23} J K^{-2}). Since subthreshold slope decreased from 8 V decade^{-1} (1 drop) to 2 V decade^{-1} (3 drops), the calculated trap density decreased from 8.9×10^{12} to 2.2×10^{12} cm^{-2}. This reduction is mainly attributed to a decrease in the number of trapping sites and corresponds well with the observed increase in field-effect mobility of IGZO TFTs. Interestingly, the V_{th} (threshold voltage) or V_{ON} (turn-on voltage) shifted toward a negative gate voltage as the drop number increased. This result could be explained in terms of the thickness-dependent increase in the electron density in the IGZO film.[19,20] Thicker IGZO films required a more negative gate bias to deplete the accumulated charge carriers. As the drop number increased to four and five drops, the diameter of the uniform central region (thickness of 30 nm) decreased abruptly (see the color contrast and height profiles of the OM images shown in Fig. 2d and e). As rectangular-type S/D electrodes were deposited onto the printed deposits prepared using four or five drops, the active channel region was defined within the pile-up region (yellow color in the OM image) as well as in the central region (cyan color in the OM image). This pile-up region was quite thick and produced irregularities in the active layer, which increased the contact resistance in the top-contact TFTs.[16] The increase in the contact resistance, in turn, triggered a high series resistance and decreased the ON current and electron mobility.

The functional properties of the TFT devices were examined by measuring the output characteristics, as shown in Fig. 4a–c and S1.† The saturation current increased as the drop number increased (from one to three drops), in accordance with the transfer curve analyses shown in Fig. 3. Regardless of the drop number, all devices showed well-resolved linear and saturation regimes, indicating that the printed IGZO deposit after IPWL sintering could be used as a switching device in display backplanes. A gate bias is repeatedly applied to a TFT device; therefore, gate bias stability is very important in TFTs. Typically, an ON current decay and a shift in the threshold voltage toward a positive bias were observed in the IGZO TFTs under a positive

Table 1 Electrical properties of IGZO TFTs with various drop numbers of IGZO solution

	Mobility ($\times 10^{-2}$ cm^2 V^{-1} s^{-1})	ON/OFF current ratio	V_{th} (V)	Subthreshold slope (V dec^{-1})
1 drop	0.9 (±0.1)	4.2 (±2.1) × 10^3	25 (±3)	8 (±1.3)
2 drops	1.5 (±0.2)	3.8 (±1.9) × 10^4	14 (±2)	6.5 (±1.5)
3 drops	10.5 (±0.8)	3.2 (±1.6) × 10^5	−15 (±3)	2 (±0.3)
4 drops	8.0 (±1.2)	1.3 (±0.7) × 10^5	5 (±3)	3.5 (±0.7)
5 drops	5.3 (±0.8)	1.6 (±0.8) × 10^5	7 (±4)	4.6 (±0.8)

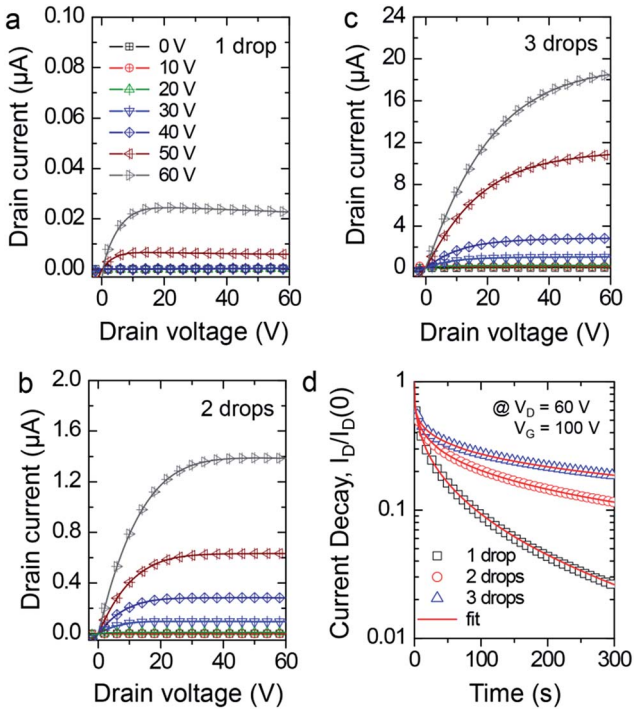

Fig. 4 Output characteristics of IGZO TFTs with various drop numbers of IGZO solution: 1 drop (a), 2 drops (b), 3 drops (c). (d) Normalized changes of currents in IGZO TFTs under the bias-stress of $V_D = 60$ V, $V_G = 100$ V.

gate bias (ON bias).[17,18,21] These observations could be explained in terms of charge trapping in the semiconductor, at the semiconductor–dielectric interface, at the S/D-semiconductor interface, and/or in the dielectric bulk. Whatever the origin, the gate bias was screened by the trapped charges, leading to an ON current decay under a prolonged ON bias. Fig. 4d shows the normalized ON current decays in the IGZO TFTs under a bias stress of $V_D = 60$ V, $V_G = 100$ V. The straight red lines indicated curve fits using the following stretched exponential equation:[22]

$$I_D(t) = I_D(0) \times \exp\left[-\left(\frac{t}{\tau}\right)^{\beta}\right]$$

where τ is the characteristic time and β is the dispersion parameter. The calculated τ and β are summarized in Table 2. The value of τ of the TFT prepared from three drops (33.5×10^5 s) was three-fold higher than the value of a TFT prepared from one drop (10.9×10^5 s), indicating that fewer traps were present in the former TFT.[23] Note that this value was directly correlated with the mean time of charge carriers to be in the mobile state. The bias stability, therefore, increased with the number of drops. Bias instability can arise from a variety of mechanisms. Charge trapping at the semiconductor and semiconductor–dielectric interface was related to the changes in the bias stability observed here. We surmised that charge trapping was closely related to an increase in the thickness of the printed IGZO deposits. Lee *et al.* examined the effects of the thickness in the active layer on the density of states in IGZO TFTs.[18] A multi-frequency method was used to measure the density of states (DOSs) in the active channel region, which was found to decease as the IGZO film thickness increased. This explanation suggests that the bias stability in a thicker film (three drops) may be enhanced because the number of trapped charges in the DOSs may decrease. Oxygen-mediated charge trapping, on the other hand, may not detract significantly from bias stability because our measurements were performed under a vacuum.[17]

Table 2 Extracted characteristic time (τ) and dispersion parameter (β) by fitting curves in Fig. 4d with the stretched exponential equation

	τ [$\times 10^5$ s]	β
1 drop	10.9	0.39
2 drops	19.0	0.28
3 drops	33.5	0.24

4. Conclusion

In summary, we developed drop-based IGZO TFTs by printing an IGZO solution using a picoliter fluidic system. IPWL sintering was used to rapidly sinter the printed IGZO deposits. The morphologies of the printed ring-like deposits depended strongly on the number of droplets printed. As the drop number increased, the thickness of the IGZO thin film increased and the pile-up region at the periphery of the deposit expanded toward the center of the deposit. The electrical properties (*i.e.*, the field-effect mobility, bias stability) of the drop-based IGZO TFTs depended strongly on the drop number. This result could be explained by considering the changes in the film thickness, both in the center and at the periphery of the ring-like deposits. Our study indicated that control over the morphology and thickness of a printed IGZO film is indispensable for optimizing the electrical properties of drop-based IGZO TFTs.

Acknowledgements

This research was supported by grants from the Basic Science Research Program (2013R1A1A2011897) and Leading Foreign Research Institute Recruitment Program (Code No. 2010-00525) through the NRF of Korea funded by the Ministry of Science, ICT & Future Planning, the Korea Institute of Science and Technology (KIST) Future Resource Research Program (2E25430).

Notes and references

1 J. Y. Kwon, D. J. Lee and K. B. Kim, *Electron. Mater. Lett.*, 2011, **7**, 1; E. Fortunato, P. Barquinha and R. Martins, *Adv. Mater.*, 2012, **24**, 2945.
2 K. Nomura, H. Ohta, A. Takagi, T. Kamiya, M. Hirano and H. Hosono, *Nature*, 2004, **432**, 488.
3 T. Kamiya, K. Nomura and H. Hosono, *Sci. Technol. Adv. Mater.*, 2010, **11**, 044305.
4 R. A. Street, T. N. Ng and R. A. Lujan, *ACS Appl. Mater. Interfaces*, 2014, **6**, 4428; K. K. Banger, Y. Yamashita,

K. Mori, R. L. Peterson, T. Leedham, J. Rickard and H. Sirringhaus, *Nat. Mater.*, 2011, **10**, 45.

5 C. H. Choi, S. Y. Han, Y. W. Su, Z. Fang, L. Y. Lin, C. C. Cheng and C. H. Chang, *J. Mater. Chem. C*, 2015, **3**, 854; K. K. Banger, R. L. Peterson, K. Mori, Y. Yamashita, T. Leedham and H. Sirringhaus, *Chem. Mater.*, 2014, **26**, 1195; J. H. Park, Y. B. Yoo, K. H. Lee, W. S. Jang, J. Y. Oh, S. S. Chae, H. W. Lee, S. W. Han and H. K. Baik, *ACS Appl. Mater. Interfaces*, 2013, **5**, 8067.

6 M. G. Kim, M. G. Kanatzidis, A. Facchetti and T. J. Marks, *Nat. Mater.*, 2011, **10**, 382; K. Everaerts, L. Zeng, J. W. Hennek, D. I. Camacho, D. Jariwala, M. J. Bedzyk, M. C. Hersam and T. J. Marks, *ACS Appl. Mater. Interfaces*, 2013, **5**, 11884.

7 B. Du Ahn, W. H. Jeong, H. S. Shin, D. L. Kim, H. J. Kim, J. K. Jeong, S. H. Choi and M. K. Han, *Electrochem. Solid-State Lett.*, 2009, **12**, H430.

8 Y. H. Kim, J. S. Heo, T. H. Kim, S. Park, M. H. Yoon, J. Kim, M. S. Oh, G. R. Yi, Y. Y. Noh and S. K. Park, *Nature*, 2012, **489**, 128.

9 T. H. Yoo, S. J. Kwon, H. S. Kim, J. M. Hong, J. A. Lim and Y. W. Song, *RSC Adv.*, 2014, **4**, 19375.

10 W. S. Han, J. M. Hong, H. S. Kim and Y. W. Song, *Nanotechnology*, 2011, **22**, 395705.

11 D. H. Lee, S. Y. Han, G. S. Herman and C. H. Chang, *J. Mater. Chem.*, 2009, **19**, 3135.

12 P. Calvert, *Chem. Mater.*, 2001, **13**, 3299.

13 G. H. Kim, H. S. Kim, H. S. Shin, B. D. Ahn, K. H. Kim and H. J. Kim, *Thin Solid Films*, 2009, **517**, 4007.

14 B. J. Larson, S. D. Gillmor and M. G. Lagally, *Rev. Sci. Instrum.*, 2004, **75**, 832.

15 D. Soltman and V. Subramanian, *Langmuir*, 2008, **24**, 2224; B. J. de Gans, P. C. Duineveld and U. S. Schubert, *Adv. Mater.*, 2004, **16**, 203.

16 Y. Li, Y. L. Pei, R. Hu, Z. M. Chen, Y. Zhao, Z. Shen, B. F. Fan, J. Liang and G. Wang, *Curr. Appl. Phys.*, 2014, **14**, 941.

17 M. G. Yun, S. H. Kim, C. H. Ahn, S. Cho and H. K. Cho, *J. Phys. D: Appl. Phys.*, 2013, **46**, 475106.

18 S. Y. Lee, D. H. Kim, E. Chong, Y. W. Jeon and D. H. Kim, *Appl. Phys. Lett.*, 2011, **98**, 122105.

19 Y. Wang, X. W. Sun, G. K. L. Goh, H. V. Demir and H. Y. Yu, *IEEE Trans. Electron Devices*, 2011, **58**, 480.

20 M. Nakata, H. Tsuji, H. Sato, Y. Nakajima, Y. Fujisaki, T. Takei, T. Yamamoto and H. Fujikake, *Jpn. J. Appl. Phys.*, 2013, **52**, 03BB04.

21 J. Raja, K. Jang, H. H. Nguyen, T. T. Trinh, W. Choi and J. Yi, *Curr. Appl. Phys.*, 2013, **13**, 246.

22 S. G. J. Mathijssen, M. Colle, H. Gomes, E. C. P. Smits, B. de Boer, I. McCulloch, P. A. Bobbert and D. M. de Leeuw, *Adv. Mater.*, 2007, **19**, 2785.

23 W. H. Lee, H. H. Choi, D. H. Kim and K. Cho, *Adv. Mater.*, 2014, **26**, 1660.